Title

Hybrid Periportal Hepatocytes Regenerate the Injured Liver without Giving Rise to Cancer

Journal

Cell, 162(4)

ISSN

0092-8674

Authors

Font-Burgada, Joan

Shalapour, Shabnam

Ramaswamy, Suvasini

et al.

Publication Date

2015-08-01

DOI

10.1016/j.cell.2015.07.026

Peer reviewed

HHS Public Access

Author manuscript

Cell. Author manuscript; available in PMC 2016 August 13.

Published in final edited form as:

Cell. 2015 August 13; 162(4): 766–779. doi:10.1016/j.cell.2015.07.026.

Hybrid Periportal Hepatocytes Regenerate the Injured Liver without Giving Rise to Cancer

Joan Font-Burgada[1,*], **Shabnam Shalapour**[1], **Suvasini Ramaswamy**[5], **Brian Hsueh**[6], **David Rossell**[7], **Atsushi Umemura**[1], **Koji Taniguchi**[1], **Hayato Nakagawa**[1,8], **Mark A. Valasek**[2], **Li Ye**[6], **Janel L. Kopp**[3,9], **Maike Sander**[3], **Hannah Carter**[4], **Karl Deisseroth**[6], **Inder M. Verma**[5], and **Michael Karin**[1,*]

[1]Laboratory of Gene Regulation and Signal Transduction, Department of Pharmacology, University of California San Diego, 9500 Gilman Drive, La Jolla, CA 92093, USA

[2]Department of Pathology, University of California San Diego, 9500 Gilman Drive, La Jolla, CA 92093, USA

[3]Department of Pediatrics and Department of Cellular & Molecular Medicine, University of California San Diego, 9500 Gilman Drive, La Jolla, CA 92093, USA

[4]Department of Medicine School of Medicine, University of California San Diego, 9500 Gilman Drive, La Jolla, CA 92093, USA

[5]Laboratory of Genetics, Salk Institute for Biological Studies, La Jolla, CA 92037, USA

[6]Departments of Bioengineering, Psychiatry, and Behavioral Sciences, Neurosciences Program, Howard Hughes Medical Institute, Stanford University, 318 Campus Drive West, Clark Center W080, Stanford, CA 94305, USA

[7]Department of Statistics, University of Warwick, Gibbet Hill Road, Coventry CV4 7AL, UK

[8]Department of Gastroenterology, The University of Tokyo, 7-3-1 Hongo, Bunkyo-ku, Tokyo 113-8655

[9]Department of Cellular & Physiological Sciences, University of British Columbia, 2350 Health Sciences Mall, Vancouver, BC V6T 1Z3, Canada

SUMMARY

[*]Correspondence: jfontburgada@ucsd.edu (J.F.-B.), karinoffice@ucsd.edu (M.K.).

AUTHOR CONTRIBUTIONS

J.F.-B. identified HybHP. J.F.-B. and M.K. conceived and designed the project. J.F.-B. performed most of the experiments and analysis. S.S., A.U., K.T., and H.N. provided assistance in experiments. S.R. and I.M.V. performed *Fah*$^{-/-}$ experiments. B.H., L.Y., and K.D. performed CLARITY. H.C. and D.R. performed RNA-seq and statistical analysis. M.A.V. provided human liver samples. J.L.K. and M.S. provided *Sox9-Cre*^{ERT} transgenic line. J.F.-B. and M.K. wrote the manuscript with all authors contributing to the writing and providing advice.

ACCESSION NUMBERS

RNA sequencing data has been deposited at SRA with accession number SRP058462 study.

SUPPLEMENTAL INFORMATION

Supplemental information includes Extended Experimental Procedures, seven figures, five movies, and a supplemental statistical analysis and can be found with this article online at http://dx.doi.org/10.1016/j.cell.2015.07.026.

Compensatory proliferation triggered by hepatocyte loss is required for liver regeneration and maintenance but also promotes development of hepatocellular carcinoma (HCC). Despite extensive investigation, the cells responsible for hepatocyte restoration or HCC development remain poorly characterized. We used genetic lineage tracing to identify cells responsible for hepatocyte replenishment following chronic liver injury and queried their roles in three distinct HCC models. We found that a pre-existing population of periportal hepatocytes, located in the portal triads of healthy livers and expressing low amounts of *Sox9* and other bile-duct-enriched genes, undergo extensive proliferation and replenish liver mass after chronic hepatocyte-depleting injuries. Despite their high regenerative potential, these so-called hybrid hepatocytes do not give rise to HCC in chronically injured livers and thus represent a unique way to restore tissue function and avoid tumorigenesis. This specialized set of pre-existing differentiated cells may be highly suitable for cell-based therapy of chronic hepatocyte-depleting disorders.

Graphical Abstract

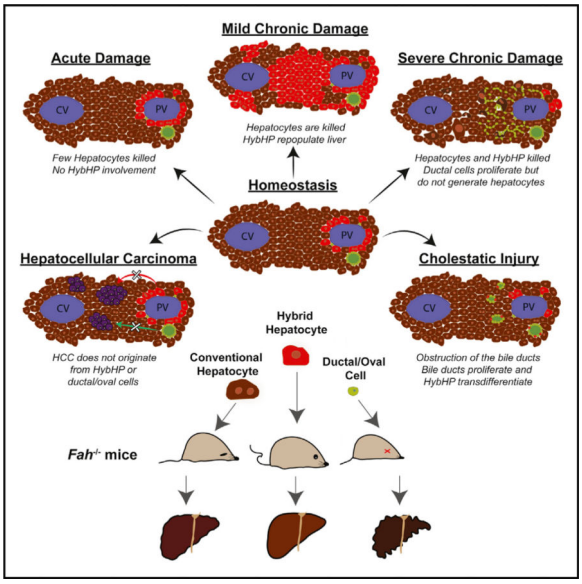

INTRODUCTION

Adult mammalian tissues rely on diverse mechanisms to maintain function and mass. Dedicated stem cell compartments that sustain normal turnover exist in highly proliferative tissues, such as skin and intestine (Blanpain and Fuchs, 2014). However, in quiescent tissues, such as liver or pancreas, the existence of stem cells and specialized niches is debatable. Furthermore, following toxic injuries, to which these tissues are highly susceptible, regenerative strategies and restorative mechanisms were proposed to include activation of dormant stem cells, transdifferentiation, metaplasia, or compensatory proliferation of mature cells (Cheung and Rando, 2013; Slack, 2007). Although liver parenchymal cells turn over slowly, the liver displays high regenerative capacity, capable of restoring 70% tissue loss within a few weeks (Michalopoulos, 2007). Given its many vital functions, especially the detoxification of harmful chemicals, the ability of liver to maintain constant mass is critical for organismal survival. During moderate and acute injuries,

differentiated hepatocytes re-enter the cell cycle, proliferate, and replenish the lost tissue, but bipotential hepatobilliary progenitors (aka oval cells) were proposed as the main source of new hepatocytes and ductal cells under conditions that interfere with hepatocyte proliferation. Such oval cells residing in a specialized niche at the junction of bile canaliculi and ducts, the canal of Hering, were postulated to serve as facultative stem cells (Miyajima et al., 2014). Yet, line-age-tracing experiments demonstrated that oval cells contribute minimally to hepatocyte restoration (Español-Suñer et al., 2012; Malato et al., 2011; Rodrigo-Torres et al., 2014; Schaub et al., 2014; Tarlow et al., 2014a; Yanger et al., 2014), implying that mature hepatocytes are responsible for tissue restitution, although it was also suggested that ductal $Lgr5^+$ stem cells can give rise to hepatocytes after in vitro propagation (Huch et al., 2013, 2015).

Compensatory proliferation has a key role in liver carcinogen-esis (Karin, 2006; Kuraishy et al., 2011). Genetic manipulations that enhance hepatocyte death, such as ablation of *Ikkβ* (Maeda et al., 2005), *Ikkγ/Nemo* (Luedde et al., 2007), or *p38α* (Hui et al., 2007; Sakurai et al., 2008), potentiate HCC development through compensatory hepatocyte proliferation. The same mechanism promotes tumorigenesis in chronic liver diseases, such as non-alcoholic steatohepatitis (NASH), that progress to HCC (Nakagawa et al., 2014b). For most cancer types, the cell of origin remains unknown, fostering intense debates about whether cancer arises from adult stem cells, transient-amplifying cells, or terminally differentiated cells that dedifferentiate. The lifetime risk of most cancers, including HCC, was proposed to correlate with the cumulative number of cell divisions in the corresponding stem cell compartment (Tomasetti and Vogelstein, 2015). It was further proposed that 2/3 of cancer risk is explainable by genetic errors that accumulate during the division of adult stem cells. Given the strong link between tissue injury, inflammation, and cancer (Kuraishy et al., 2011), one can assume that also in liver, the cells with the highest replicative potential are the ones that give rise to HCC. Indeed, oval cells were suggested as likely HCC progenitors (Sell and Leffert, 2008), and we identified HCC progenitor cells (HcPC) induced by diethylnitrosamine (DEN) that resemble oval cells in their transcriptomic profile (He et al., 2013). However, because DEN has to undergo metabolic activation by CYP2E1, which is expressed only in fully differentiated zone 3 hepatocytes (Kang et al., 2007), we suggested that HcPC are not derived from oval cells (He et al., 2013). Nonetheless, oval cells that expand in NASH (Richardson et al., 2007) are still thought of as likely HCC progenitors.

Unresectable HCC and end-stage liver diseases can only be treated by liver transplantation, but the availability of appropriate donor tissue is limited, necessitating a search for alternatives. One possibility is transplantation of adult liver stem cells, but despite extensive research, the existence and identity of such cells remains elusive (Miyajima et al., 2014). The safety of donor cells is another issue, given the possible link to HCC development. Notably, human ductal cells can be expanded and differentiated in vitro to transplantable hepatocytes (Huch et al., 2015; Schmelzer et al., 2007), but given the low efficiency of this approach, additional solutions are needed. We now describe a distinct population of hepatocytes that exist at the periportal region of the uninjured liver. Because these cells express several bile-duct-enriched genes, including low amounts of *Sox9*, they were named hybrid hepatocytes (HybHP). We show that HybHP are highly efficient in repair of livers

deficient in healthy hepatocytes, but despite their high regenerative capacity, they do not give rise to HCC in three independent models. Thus, the cells with the highest proliferative potential in a given tissue may not necessarily be the ones that give rise to cancer.

RESULTS

Hybrid Periportal Hepatocytes with High Regenerative Capacity

The portal area may be the organizing center for liver repair, harboring putative stem cell niches (Kuwahara et al., 2008). We examined the regenerative capacity of cells in this region using transgenic mice expressing GFP from the *Sox9* promoter, which is primarily active in bile duct cells (BD) and bipotential hepatobilliary progenitors. Immunofluorescence (IF) analysis indicated that ductal $CK19^+$ cells showed high GFP expression, but other cells located in the limiting plate around the bile duct and the portal vein (PV) expressed low amounts of GFP (Figures 1A–1C). These cells were negative for the ductal marker CK19 (Figure 1B) and positive for the hepatocyte marker HNF4α (Figure 1C), suggesting that they are hepatocytes. These periportal hepatocytes comprise 4.53% ± 0.24% of all hepatocytes (Figure 1A, based on 7,390 GFP^+ hepatocytes out of 163,292 hepatocytes, n = 3). GFP^+ periportal hepatocytes are stable in both males and females throughout their lifetimes (Figure S1A).

To examine the regenerative and differentiative capacity of GFP^+ periportal hepatocytes and determine whether they differ from *Sox9-GFP*-negative hepatocytes, we used a *Sox9-Cre*^{ERT} transgenic line suitable for labeling low SOX9-expressing cells (see Experimental Procedures). In such *Sox9-Cre*^{ERT}*;R26R*^{YFP} mice, some ductal cells ($CK19^+$ $HNF4\alpha^-$) were YFP labeled without tamoxifen administration (Figure 1D), suggesting leaky Cre^{ERT} nuclear translocation. However, almost no hepatocytes ($CK19^-$ $HNF4\alpha^+$) expressed YFP without tamoxifen (Figure 1D; 1,427 $CK19^+/YFP^+$ out of 1,434 YFP^+ cells, n = 2). YFP^+ $CK19^-$ $HNF4\alpha^+$ periportal hepatocytes appeared after a single 5 mg/kg tamoxifen dose at postnatal day 10 (P10) (Figure 1E), but more cells were found after 100 mg/kg tamoxifen, which labeled 2.3% ± 0.15% of total hepatocytes with YFP, at an estimated efficiency of 51.4% (Figure 1F; 4,968 YFP^+ hepatocytes out of 217,975 hepatocytes, n = 3), mirroring what was observed with the *Sox9-GFP* transgene (Figures 1A–1C) and inconsistent with the SOX9 expression pattern of wild-type (WT) mice given high tamoxifen doses (Carpentier et al., 2011). YFP^+ periportal hepatocytes remained stable for at least 9 months (Figure S1B). Ductal cell labeling efficiency after a single 100 mg/kg tamoxifen injection at P10 was 95.4% (Figure 1F; 5,321/5,577 cells, n = 3). Based on their elevated basal *Sox9* promoter activity and expression of other ductal markers (see below), we named these cells HybHP. The exact location of HybHP within the portal tract (PT), relative to the canals of Hering, was determined by CLARITY analysis (Chung et al., 2013). Because endogenous *Sox9-GFP* and *R26R*^{YFP} fluorescent signals were too dim, we chose *R26tdTomato* due to its brightness (Figure S1C). Clarified livers from tamoxifen-treated *Sox9-Cre*^{ERT}*;R26R*^{tdTomato} mice were stained with CK19 antibody to delineate the ductal tree and imaged. HybHP were found to wrap around the PV and contact the intricate mesh formed by the bile ducts and their terminal branches, which form the canals of Hering (Figures 1G and S1D and Movies S1, S2, S3, and S5). Not all HybHP were attached to BD (Figure 1H and Movie S4).

Next, we analyzed the behavior of YFP^+ HybHP during the regeneration period after different types of liver injury. We gave mice CCl_4 to induce pericentral damage (Wong et al., 1998). A single CCl_4 dose (acute—1 μl/gr) in *Sox9-Cre^{ERT};R26R^{YFP}* mice resulted in minor HybHP expansion after 4 weeks (Figure 2A; 10,654 HybHP out of 239,888 hepatocytes, to 8.6%, n = 3). However, repetitive administration of a lower CCl_4 dose (chronic—0.5 μl/gr), which gives rise to fibrosis (Wong et al., 1998) without oval cell expansion (Español-Suñer et al., 2012; Grompe, 2014; Rodrigo-Torres et al., 2014; Tarlow et al., 2014a; Yanger et al., 2014), led to 34.5% ± 2.2% of all hepatocytes being derived from YFP^+ HybHP, with most cells extending along hepatic cords from the periportal region to the CV (Figure 2B; 5,213 YFP^+ out of 14,947 hepatocytes from 41 independent areas, n = 2). Given the estimated labeling efficiency of 51.4%, HybHP contributed to 67% of new hepatocytes. Littermates not receiving CCl_4 did not show HybHP expansion (Figure 2C). Expanding YFP^+ hepatocytes that reached the CV expressed glutamine synthetase (GS), a marker of zone 3 hepatocytes, indicating that HybHP produce fully differentiated and functional hepatocytes, whose metabolic profiles match their locations along the portal-central axis (Figure S2B).

We also used *MUP-uPA* transgenic mice, which undergo liver damage due to ER stress induced by overexpression of urokinase-type plasminogen activator (uPA) in hepatocytes (Nakagawa et al., 2014b; Weglarz et al., 2000). *MUP-uPA* mice first display liver damage at 3 weeks of age; it peaks at 5 weeks and dissipates by 13 weeks (Weglarz et al., 2000). Without tamoxifen, 99.9% YFP^+ cells remained $CK19^+$ in 9-week-old *Sox9-Cre^{ERT};MUP-uPA;R26R^{YFP}* mice (Figure 2D; 4,838 $CK19^+/YFP^+$ cells out of 4,842 YFP^+ cells, n = 3), suggesting that neither ductal nor oval cells differentiated into hepatocytes. However, after administration of 100 mg/kg tamoxifen at P10, YFP^+ HybHP made a substantial contribution to new hepatocytes, forming clones that expanded out of all portal areas, accounting for 20% of hepatocytes at 5–6 weeks of age (Figures 2E and S2A). In mice analyzed 5–6 weeks later, some YFP^+ clones disappeared and were replaced by ductular reactions, but the surviving clones were large and contacted the corresponding CV (Figures 2F and S2A). HybHP-derived clones covered 49.6% of CV-PT areas in the corresponding portal lobules (49.6% ± 4.5%, 21 independent portal lobules, n = 3) after 9 weeks, suggesting that HybHP can repopulate the entire parenchyma in *MUP-uPA* mice. Newly labeled hepatocytes reaching the CV expressed GS (Figure S2C).

We further examined the contribution of HybHP to newly produced hepatocytes with an independent genetic tool. We reasoned that by labeling hepatocytes randomly, it should be possible to compare the clonal behavior of HybHP to that of parenchymal hepatocytes. The *TTR-Cre^{ERT}* driver led to sparse and random labeling of hepatocytes (Figures S3A and S3B). In *TTR-Cre^{ERT};R26R^{YFP};MUP-uPA* mice treated with 100 mg/kg tamoxifen at P10 and analyzed 4 weeks later, some labeled hepatocytes produced proliferative YFP^+ clones, but most of the original YFP^+ hepatocytes were eliminated by ongoing liver damage (Figures S3C and S3D). Nonetheless, surviving YFP^+ hepatocytes gave rise to expanding clones that originated from the PT, confirming that the distribution of damage-repairing cells is not random and is consistent with what was seen above (Figure S3D). When *TTR-Cre^{ERT};R26R^{YFP}* mice were subjected to chronic CCl_4 treatment, the observed pattern of

expanding YFP^+ clones was also consistent with a PT origin (Figures S3E and S3F). The absence of oval cell contribution to new hepatocytes in *MUP-uPA* mice was confirmed using the *CK19-Cre^{ERT}* driver, which labels BD and oval cells (Figure S3G; 1,333 $CK19^+/YFP^+$ out of 1,333 YFP^+ cells, n = 3). We also gave tamoxifen (100 mg/kg) to *Sox9-Cre^{ERT};R26R^{YFP}* mice and fed them with choline-deficient, ethionine-supplemented (CDE) diet, which leads to extensive liver damage with high mortality (Akhurst et al., 2001). In these mice, most HybHP were destroyed, and vast oval cell expansion was seen (Figure S3H), suggesting that when HybHP are compromised, oval cells take over but do not give rise to new hepatocytes.

Clonally Labeled HybHP Produce New Hepatocytes and Transdifferentiate into Duct Cells

To further examine HybHP participation in regeneration after chronic liver damage, we used a system in which only HybHP are specifically and clonally labeled. We crossed *Sox9-Cre^{ERT}* and *NZG* mice, which contain a *loxP*-flanked STOP cassette up-stream of a nuclear targeted *LacZ* marker as well as a down-stream GFP marker whose expression is prevented by the *Frt*-flanked *LacZ* cassette itself (Figure 3A). Tamoxifen administration to heterozygous mice labeled SOX9-expressing cells (duct cells and HybHP) with nuclear LacZ, but not a single cell was ever found GFP positive. (Figure 3B). To specifically label HybHP we took advantage of the fact that adenovirus (Nakagawa et al., 2014a) or AAV-TBG (Yanger et al., 2013) only target hepatocytes. Infection of *Sox9-Cre^{ERT};NZG* mice, previously treated with tamoxifen, with either adenoviruses or AAV expressing FLPo recombinase that excises the *LacZ* cassette resulted in GFP labeling of some HybHP (Figure 3C) that were $CK19^-$ (551 cells, n = 3) and $HNF4\alpha^+$ (323 cells, n = 3), confirming labeling specificity (Figures 3D and 3E). Three weeks after viral infection and 5 weeks after initial tamoxifen injection, different groups of mice were allocated to determine the clonal behavior of HybHP after CCl_4 treatment. Although no significant response was observed in mice treated with an acute or a single CCl_4 dose, in which mainly single HybHP-derived hepatocytes were found, multicellular clones expanding from the PT were observed after six CCl_4 injections. After six more injections, clones containing > 5 hepatocytes were readily detected, with several clones contacting the corresponding CV with more than 20 cells (Figures 3F and 3G), confirming what was observed with the single reporter system and further establishing the role of HybHP in repopulating the liver after chronic hepatocyte damage.

Biphenotypic hepatocytes, also known as ductular hepatocytes, which express ductal markers and give rise to ductal cells, were reported in cholestatic liver injury models (Tanimizu et al., 2014; Tarlow et al., 2014b; Yanger et al., 2013). Hepatocyte-derived proliferative ducts (HepPD) can also be isolated from 3,5-dicarbethoxy-1,4-dihydrocollidine (DDC) diet-fed *Fah$^{-/-}$* mice that were transplanted with normal hepatocytes (Tarlow et al., 2014b). Given that HybHP are present in the un-injured liver and express some bile duct genes, we postulated that after cholestatic liver injury they may give rise to true ductal cells. We tested this possibility with the *NZG* dual recombinase system that specifically labels HybHP, inducing cholestatic injury with DDC-containing diet. After 6 weeks of DDC feeding, most HybHP underwent pronounced morphological changes, acquiring smaller cell and nuclear sizes and strong expression of SOX9 and osteopontin (OPN), a ductal marker

(Figure 4). Ten percent of HybHP lost HNF4α expression, and 2.5% of these cells incorporated into bile ducts and showed strong CK19 expression (Figure 4). These results are consistent with conversion of pre-existing ductal cells into oval cells during cholestatic injury but also suggest that a minor proportion of oval cells arise from trans-differentiating hepatocytes, which most likely are identical to HybHP. Fittingly, tamoxifen-treated *Alb-Cre^{ERT2};R26R^{YFP}* mice consistently contained YFP^{+} ductal cells in the absence of any damage (Figure S3I), suggesting that the hypothesis that DDC-induced oval cells arise mainly from mature hepatocytes should be re-evaluated.

HybHP Exhibit a Unique Transcriptome

We isolated HybHP, conventional hepatocytes (cHP), and BD by sorting collagenase digests of tamoxifen-treated *Sox9-Cre^{ERT};R26R^{tdTomato}* livers (Figures 5A, S1C, and S4). YFP was unsuitable for these experiments because it did not distinguish labeled cells from endogenous autofluorescent cells (Figure S4A). The three populations were subjected to RNA-seq analysis, which indicated that the HybHP transcriptome was similar to the cHP transcriptome and that both cHP and HybHP differed extensively from BD (Figure S5A). However, HybHP diverged from cHP by 490 genes, of which 233 were upregulated and 257 were downregulated (Figure 5B). Statistical analysis indicated that the observed differences were not the result of biological or technical noise and did not originate from a mixture of BD + cHP (Figure S6). The differentially expressed genes were subdivided into four classes: (1) genes that are upregulated in both HybHP and BD relative to cHP; (2) genes whose expression is lower in HybHP than in cHP or BD; (3) genes whose expression is higher in HybHP than in cHP or BD; and (4) genes that are downregulated in both HybHP and BD relative to cHP (Figure 5B). Classes 1 and 4 comprised 64% of the differentially expressed genes and are shared with BD (Figure 5C). The probability of obtaining such results by mere chance was negligible ($p < 10^{-49}$), indicating that HybHP are distinct hepatocytes with some BD characteristics. Inspection of lineage-specific markers confirmed that HybHP express ductal markers, including *Sox9* and *Opn*, which are barely expressed by cHP (Figure 5D). Coincidentally, major hepatocyte fate determinants, such as *Hnf1α* and *Hnf4α*, were equally expressed by HybHP and cHP, but other BD markers such as *Hnf1β* and *EpCam* were hardly upregulated (Figure 5D). Functional classification revealed that genes belonging to class 1, which are upregulated in both HybHP and BD, are mostly involved in cell adhesion, interactions with extra-cellular matrix (ECM), and processes related to morphogenesis and tube formation (Figure S5B). The intimate interaction between HybHP and BD may require homotypic interactions mediated by such molecules, which are expressed at very low levels in cHP. IF analysis of Sox9-GFP liver sections revealed that HybHP express low levels of SOX9 and OPN (Figure 5E). Similar signals were detected in liver sections from WT mice (Figure S5C). Normal human liver contains periportal hepatocytes that co-express HNF4α and HNF1β (Isse et al., 2013). Importantly, hSOX9 and hOPN were expressed by some periportal hepatocytes in human liver (Figure 5F), suggesting that human liver also contains HybHP.

Class 4 genes, which are downregulated in both HybHP and BD, are mainly involved in oxidative drug metabolism (Figure S5B). These genes are expressed at high levels in cHP, and their downregulation may explain why HybHP are less sensitive to damage caused by

metabolic activation of toxic chemicals, such as CCl_4, which is mainly metabolized by CYP2E in zone 3 hepatocytes (Wong et al., 1998). Class 2 and 3 genes are those with the lowest and highest expression in HybHP relative to the other populations, respectively. Class 3 genes did not show enrichment for any particular functional category, suggesting that these genes are involved in many diverse functions. IF staining for the products of two such genes, *Agxt2l1* and *Aqp4*, revealed that they are expressed by zone 1 hepatocytes (Figure S5D). Given that our analysis compared HybHP to bulk hepatocytes depleted of HybHP, it is likely that genes that are highly expressed by zone 1 hepatocytes would appear upregulated in HybHP. Intriguingly, class 2 genes exhibit statistically significant enrichment for processes related to innate and adaptive immunities (Figure S5B), suggesting that HybHP are less likely to respond to damage-associated molecular patterns (DAMPs), pathogen-associated molecular patterns (PAMPs), and other inflammatory stimuli that trigger the acute phase response. Although some class 2 genes are also expressed in Kupffer cells, the purity of cHP is very high (> 97%), and only a small number of $CD45^+$ cells was present in this population (data not shown). Furthermore, some of these genes, for instance *Tlr5* and *Tlr8*, are not expressed in Kupffer cells (Lavin et al., 2014). Altogether, these data suggest that the HybHP transcriptome is a hybrid of the HP and BD transcriptomes with a few immune response genes that are downregulated relative to cHP (Figure S5E).

Transplanted HybHP Display High Regenerative Capacity

The high regenerative potential and plasticity of HybHP make them attractive candidates for liver disease cell therapy. We examined this possibility using $Fah^{-/-}$ mice, which due to FAH (fumarylacetoacetate hydrolase) deficiency undergo spontaneous liver damage upon withdrawal of NTBC (2-nitro-4-trifluoromethylbenzoyl–1,3-cyclo-hexanedione) and, if left untreated, succumb to fatal liver failure within 1–2 months (Grompe et al., 1995). HybHP ($tdTomato^+$) and cHP ($tdTomato^-$) from tamoxifen-treated $Sox9\text{-}Cre^{ERT};R26R^{tdTomato}$ mice and oval cells ($tdTomato^+$) from CDE diet-fed animals of the same genotype were transplanted (45,000 sorted cells of each type) into spleens of $Fah^{-/-};Rag2^{-/-};Il2rg^{-/-}$ recipient mice (Bissig et al., 2007), which were subsequently withdrawn from NTBC for 3 weeks, put on NTBC for 1 week, and kept 4 more weeks without NTBC. Oval cells generated hardly any $tdTomato^+$ clones, but HybHP-transplanted mice showed numerous $tdTomato^+$ clones in all liver lobules covering a large part of the surface (Figure 6A). Due to higher autofluorescence of cHP relative to the $Fah^{-/-}$ background, we also detected clones derived from these cells. Oval cells retained ductal morphology and did not express FAH, but HybHP clones consisted of $FAH^+/tdTomato^+$ hepatocytes, and cHP-generated clones were $FAH^+/tdTomato^-$ (Figure 6B). Clonal area measurements on the liver surface showed that HybHP were superior to cHP, generating clones that were two times larger (Figure 6C, upper graph). Measurement of clonal areas in histological sections yielded similar results, with HybHP-generated clones being 2.5-fold larger than cHP-generated clones (Figure 6C, lower graph). Of note, human cirrhotic livers lose metabolic zonation resulting in diffuse GS expression throughout the parenchyma (Fleming and Wanless, 2013). GS staining of liver sections from HybHP-transplanted mice showed that expanding clones exhibited normal zonation with few GS^+ cells near the CV (Figure 6D). These results underscore the higher repopulation potential of HybHP and indicate that HybHP progeny acquire the correct metabolic profile according to their location along the portal-central axis. To further assess

the therapeutic potential of HybHP, we followed another cohort of transplanted mice for a longer time. Due to the limited number of HybHP that were available for these experiments, we only transplanted 14,000–50,000 cells, much less than the 500,000–1,000,000 cells commonly used in such studies. At the end of the study, we found that all HybHP-transplanted animals were still alive, whereas 90% of control animals and more than 50% of cHP-transplanted mice had died (Figure 6E).

Neither HybHP nor Oval Cells Give Rise to HCC

In many experimental models of hepatic carcinogenesis, oval cell responses precede the emergence of neoplasia, as observed in humans where ductular reactions precede HCC in cirrhotic livers (Roskams, 2006). Such observations were interpreted to suggest that oval cells could initiate a large fraction of liver cancers (Alison et al., 2009). Given the high proliferation rate of HybHP during chronic liver injury, HybHP could serve as an alternative origin for HCC. To examine this point, we traced HybHP and oval cells in three independent mouse models of HCC: DEN-induced HCC (Maeda et al., 2005), *MUP-uPA* mice fed with high-fat diet (HFD) (Nakagawa et al., 2014b), and the STAM model of diabetes-promoted HCC (Fujii et al., 2013), using the *Sox9-Cre*^{ERT}*;R26R*^{YFP} reporter system. Whereas DEN is metabolically activated in pericentral/zone 3 hepatocytes and does not induce oval cell expansion, consumption of HFD, which induces liver damage and compensatory proliferation in both *MUP-uPA* and STAM mice, gives rise to substantial oval cell proliferation (Figure S7). Cell labeling in all three cases was conducted prior to induction of any cellular damage or carcinogenic insult using 100 mg/kg tamoxifen (Figure 7A), which labels HybHP and ductal cells with 51% and 95% efficiency, respectively. No YFP^{+} cells were detected in well-developed tumor nodules and hyperproliferative lesions (Figures 7B–7D, n = 106 HCC nodules from 9 DEN-treated mice, n = 79 HCC nodules in 7 MUP-uPA + HFD mice, and n = 62 HCC nodules in 5 STAM mice). These results and their corresponding binomial distributions suggest that it is very unlikely that HybHP or ductal cells are the preferred origins for HCC in these models ($p < 10 \times 10^{-10}$). We determined the 95% credibility intervals (C.I.) (Beta [1,1] prior distribution) for the expected percentage of HybHP- or ductal cell-derived tumors that are compatible with our experimental data. For HybHP, the obtained C.I. (DEN, 0%–5.3%; MUP-uPA + HFD, 0%–7.2%; and STAM, 0%–9%) suggest that even if HybHP were a potential source for HCC, the majority of tumors (> 91%) did not originate from them. Due to the higher labeling efficiencies for duct cells, the obtained C.I. values (DEN, 0%–2.8%; MUP-uPA + HFD, 0%–3.9%; and STAM, 0%–4.9%) were even more definitive in ruling out ductal cells as the HCC origin. These results strongly suggest that HCC in these models is derived from differentiated hepatocytes.

DISCUSSION

Detoxification of noxious chemicals and toxic metabolites is an important function of the vertebrate liver. Xenobiotic metabolism, however, increases the propensity of the liver to undergo toxic damage, which can result in rapid loss of tissue mass, a potential handicap that is prevented by maintaining high regenerative capacity. Our results indicate that the major strategy for restoring liver mass and function after chronic hepatocyte injury depends on the proliferation of HybHP, a specialized type of hepatocyte that barely expresses drug-

metabolizing genes. This property and other metabolic features protect HybHP from toxic injury and reduce the likelihood that they will give rise to cancer, despite their high proliferative potential.

HybHP as Distinct Hepatocyte Subpopulation

Hepatocyte diversity has been long appreciated, especially in the context of metabolic zonation across the portal-central axis (Jungermann and Katz, 1989). However, it has been difficult to functionally examine different hepatocyte populations under physiological conditions. Using the ductal transcription factor Sox9 as a marker, we identified a subpopulation of periportal hepatocytes located at the limiting plate, which express low amounts of SOX9 and normal amounts of HNF4α. These cells were named HybHP, based on their expression of hepatocytespecific genes along with a small number of signature genes of BD. Many of these genes are functionally related to cell adhesion and tubule formation, suggesting that HybHP and BD may originate from a common embryonic progenitor located at the ductal plate (Carpentier et al., 2011). Such a progenitor may give rise to mature BD and HybHP that remain connected via homotypic interactions (Miyajima et al., 2014). This close proximity should expose HybHP to factors, for instance Notch ligands, which are expressed by ductal cells and allow HybHP to acquire a partial ductal character. Importantly, many of the genes that are underexpressed in HybHP relative to cHP are involved in drug metabolism and immune responses, categories that represent specialized functions of more differentiated hepatocytes that allow them to detoxify xenobiotics and products of the gastrointestinal microbiome that reach the liver via the portal circulation. Underexpression of such genes may make HybHP more resistant to toxic insults and inflammatory stress. At this point, however, we do not know whether this specific transcriptomic profile is hardwired or is modulated by the specific location at which HybHP reside, especially considering the fact that once HybHP progeny approach the CV, they upregulate certain metabolic genes. Cells that resemble HybHP, based on weak expression of SOX9 and OPN, are also present in human liver, but their functional characterization will require development of improved isolation techniques.

HybHP—A New Framework for Understanding Liver Regeneration

Liver regeneration has been extensively studied in the context of partial hepatectomy, in which all liver cells undergo limited rounds of cell division to restore organ mass. However, studies of injury-induced regeneration gave rise to conflicting hypotheses, such as the streaming liver (Fellous et al., 2009; Furuyama et al., 2011), the liver stem cell (Dorrell et al., 2011), and the highly controversial oval cell concept (Miyajima et al., 2014). Although recent studies show that oval cells do not generate hepatocytes (Espa ñol-Suñer et al., 2012; Malato et al., 2011; Rodrigo-Torres et al., 2014; Schaub et al., 2014; Tarlow et al., 2014a; Yanger et al., 2014), cultured BD were found capable of giving rise to hepatocytes (Huch et al., 2013, 2015). The discovery of HybHP allows us to propose an integrative model that reaffirms the fundamental role of the portal-central axis in liver physiology, with the PT as the source of cells responsible for the majority of parenchymal regeneration. Although acute insults are rapidly resolved by surviving hepatocytes, we suggest that the repair of chronic hepatocyte damage requires the proliferation of HybHP. We postulate that HybHP are mainly activated under conditions when the damaged parenchyma can be more efficiently

repopulated by hepatocytes that originate from the limiting plate. When too many hepatocytes are continuously destroyed and the highly complex network of hepatic sinusoids and bile canaliculi is compromised, the most effective way to properly repair such injuries is to induce the expansion of hepatocytes that are already connected to BD, a task that can be most easily fulfilled by HybHP. However, when liver damage is extensive and sustained and HybHP are killed, they can no longer contribute to the regenerative process. Under such conditions, the oval cell response is activated, but oval cells are incapable of differentiating into hepatocytes, and the logic underlying their expansion remains obscure. One possible function for oval cells could be restoration of the bile canaliculi network and liver polarity. Supporting these lines, inking the ductal tree has allowed visualization of its structure in different models of liver injury with oval cell expansion (Kaneko et al., 2015). Such studies show that oval cells are extensions of the pre-existing ductal tree, further challenging the view that oval cells are progenitor cells that seed the parenchyma to generate new hepatocytes.

HybHP and HCC

Our results suggest that despite their high regenerative and proliferative potential, HybHP do not give rise to HCC in two models in which HCC arises in a liver that is chronically damaged by steatohepatitis. Likewise, HybHP do not give rise to HCC in a liver that has been acutely challenged by DEN injection. Thus, not all cells that undergo many rounds of division will accumulate a sufficient number of mutations and give rise to cancer (Tomasetti and Vogelstein, 2015). The inability of HybHP to give rise to HCC in these models is unlikely to be due to intrinsic resistance to oncogenic transformation, as most cells can be transformed upon oncogene activation or loss of tumor suppressors. Most likely, the metabolic properties of HybHP and their constellation of signaling molecules make them unable to participate in HCC initiation in the three models that were examined. In the case of DEN, it is well established that metabolic activation of this pro-carcinogen depends on CYP2E1, which is only expressed in zone 3 hepatocytes (Kang et al., 2007). Zone 3 hepatocytes are also the cells that are killed by DEN exposure due to generation of reactive oxygen species (ROS) during its metabolism (Maeda et al., 2005). In the case of *MUP-uPA* and STAM mice, HCC development depends on HFD consumption (Fujii et al., 2013; Nakagawa et al., 2014b), which promotes de novo lipogenesis and ROS generation through fatty-acid oxidation (Nakagawa et al., 2014b), properties encoded by class 4 genes that are highly expressed in fully differentiated hepatocytes. These findings suggest that the mere number of cell divisions to which a given cell type is subjected may not be the rate-limiting factor in determining its oncogenic potential. In addition to high proliferative potential, a cancer progenitor should possess unique metabolic and signaling properties that are compatible with oncogenic transformation.

HybHP as a Treatment for Chronic Liver Disease

Chronic liver disease remains the leading cause of liver transplantation, a highly expensive procedure and a prominent cause of morbidity and mortality. Cell transplantation has been proposed as an alternative to liver transplantation, but the ideal donor cell remains to be identified. Liver stem cells, cultured ductal cells, and their derivatives were proposed (Huch et al., 2013, 2015; Miyajima et al., 2014). Fetal liver progenitor cells also hold promise for

transplantation therapy, but concerns were raised about their safety and methods of isolation (Kisseleva et al., 2010). Induced pluripotent stem cells (iPSC) can be converted into hepatocytes, but the repopulation potential and functional recovery of such cells are inferior to those of cHP (Forbes et al., 2015). Furthermore, the tumorigenicity of hepatocytes derived from iPSC has not been ruled out. To the best of our knowledge, HybHP exhibit the highest regenerative capacity of all cells introduced into the *Fah*$^{-/-}$ mouse liver, and thus, we suggest that HybHP are ideal candidates for liver disease cell therapy. However, the future clinical use of HybHP will depend on ease of isolation and the development of suitable culture systems for continuous propagation and massive expansion.

EXPERIMENTAL PROCEDURES

Mice

Mouse studies were performed in accordance with NIH guidelines for the use and care of laboratory animals and approved by the UCSD Institutional Animal Care and Use Committee, S00218. Tamoxifen (Sigma-Aldrich) was dissolved in corn oil and subcutaneously (s.c.) injected to mice before the induction of any damage or experimental intervention with a wash out period of at least 1 week.

Immunofluorescence Analysis

Mice were intra-cardially perfused with Zn-Formalin (Polysciences), and excised livers further fixed overnight in Zn-Formalin. Livers were washed with PBS and incubated for 2 hr with 100 mM Tris (pH 9.4), 10 mM DTT. Livers were washed stepwise with PBS-15% and 30% sucrose at 4°C embedded in Tissue Tek OCT compound (Sakura Finetek) and kept frozen. Tissue blocks were cut with a cryostat to 8 μm sections. Slides were washed in PBS, and antigen retrieval was performed with citrate (pH 6) buffer at 96°C for 1 hr. After cooling and washing the slides with PBS, they were incubated with PBS-0.1% Triton X-100 for 20 min. After extensive washing with PBS, the slides were blocked with PBS-0.1% Tween-2% Donkey serum for 30 min. Antibodies were diluted in the same blocking buffer and incubated at 4°C overnight. Slides were washed three times with PBS-0.1% Tween and incubated with corresponding secondary antibodies diluted in blocking solution for 2 hr, followed by 3× PBS-0.1% Tween and 2× PBS washes. Slides were washed further with deionized water and 70% ethanol prior to incubation with 0.1% Sudan Black (Sigma) in 70% ethanol for 20–30 min. Extensive washing with PBS-0.2% Tween was performed before incubating the slides with DAPI for nuclear staining and mounting with Mowiol. Imaging was performed with a Zeiss Axioimager2 and Hamamatsu Nanozoomer. Images were processed using Zeiss ZEN and NDPview Hamamatsu software.

Liver Perfusion, Flow Cytometry, and Cell Sorting

For flow cytometry analysis, liver single cells were isolated by two-step collagenase digestion and differential centrifugation. Single-cell suspensions were analyzed using HNF4α (Santa Cruz #sc-6556) and CK19 (TROMAIII Developmental Studies Hybridoma Bank) antibodies. Donkey anti-goat alexa-647 and donkey anti-goat alexa-405 (Molecular Probes, Invitrogen) were used as secondary antibodies. For intracellular staining, Transcription Factor Staining Kit (BD Biosciences) was used. Fixable Viability Dye eFlour

780 Dye or eFlour 506 was used for exclusion of dead cells (eBioscience). Samples were measured on a CyAn ADP flow cytometer (Beckman Coulter) and analyzed with FlowJo.8 software (Tree Star) or a BD Influx for cell sorting.

Supplementary Material

Refer to Web version on PubMed Central for supplementary material.

ACKNOWLEDGMENTS

We thank Drs. D. Brenner, T. Kissileva, M. Grompe, and G. Napolitano for comments, M. Vasseur-Cognet for *TTR-Cre*^{ERT} mice, P. Chambon for *Alb-Cre*^{ERT}, and W. Sandgren for *MUP-uPA* mice. Technical support was provided by the UCSD Neuroscience Microscopy Shared Facility (P30 NS047101), the IGM Genomics Center, human stem cell core facility, and the Vector Core Developmental Lab. J.F.-B. was supported by CIRM Training Grant II (TG2-01154); A.U. by a Global Grant Scholarship from The Rotary Foundation; K.T. by a postdoctoral fellowship for Research Abroad, Research Fellowship for Young Scientists from the JSPS, and the Uehara Memorial Foundation Fellowship; S.S. by the DFG and a CRI-Irvington fellowship; and H.N. by the Japanese Society of Gastroenterology, The Tokyo Society of Medical Sciences, and Kanae Foundation. Research was supported by NIH grants CA118165 and CA155120 and the Superfund basic research program (ES010337) to M.K., who holds the Ben and Wanda Hildyard Chair for Mitochondrial and Metabolic Diseases and is an ACS Research Professor, and NIH grants HL053670 and AI048034, Cancer Ctr Core Grant (P30 CA014195-38), the Frances C. Berger Foundation, and Leona M. and Harry B. Helmsley Charitable Trust grant 2012-PG-MED002 to I.M.V. M.S. was supported by NIH grants DK078803 and DK068471, and J.L.K. by NIH grant F32CA136124 and an Advanced Postdoctoral Fellowship from the JDRF.

REFERENCES

Akhurst B, Croager EJ, Farley-Roche CA, Ong JK, Dumble ML, Knight B, Yeoh GC. A modified choline-deficient, ethionine-supplemented diet protocol effectively induces oval cells in mouse liver. Hepatology. 2001; 34:519–522. [PubMed: 11526537]

Alison MR, Islam S, Lim S. Stem cells in liver regeneration, fibrosis and cancer: the good, the bad and the ugly. J. Pathol. 2009; 217:282–298. [PubMed: 18991329]

Bissig K-DD, Le TT, Woods N-BB, Verma IM. Repopulation of adult and neonatal mice with human hepatocytes: a chimeric animal model. Proc. Natl. Acad. Sci. USA. 2007; 104:20507–20511. [PubMed: 18077355]

Blanpain C, Fuchs E. Stem cell plasticity. Plasticity of epithelial stem cells in tissue regeneration. Science. 2014; 344:1242281. [PubMed: 24926024]

Carpentier R, Suñer RE, van Hul N, Kopp JL, Beaudry JB, Cordi S, Antoniou A, Raynaud P, Lepreux S, Jacquemin P, et al. Embryonic ductal plate cells give rise to cholangiocytes, periportal hepatocytes, and adult liver progenitor cells. Gastroenterology. 2011; 141:1432–1438. e1–e4. [PubMed: 21708104]

Cheung TH, Rando TA. Molecular regulation of stem cell quiescence. Nat. Rev. Mol. Cell Biol. 2013; 14:329–340. [PubMed: 23698583]

Chung K, Wallace J, Kim SY, Kalyanasundaram S, Andalman AS, Davidson TJ, Mirzabekov JJ, Zalocusky KA, Mattis J, Denisin AK, et al. Structural and molecular interrogation of intact biological systems. Nature. 2013; 497:332–337. [PubMed: 23575631]

Dorrell C, Erker L, Schug J, Kopp JL, Canaday PS, Fox AJ, Smirnova O, Duncan AW, Finegold MJ, Sander M, et al. Prospective isolation of a bipotential clonogenic liver progenitor cell in adult mice. Genes Dev. 2011; 25:1193–1203. [PubMed: 21632826]

Español-Suñer R, Carpentier R, Van Hul N, Legry V, Achouri Y, Cordi S, Jacquemin P, Lemaigre F, Leclercq IA. Liver progenitor cells yield functional hepatocytes in response to chronic liver injury in mice. Gastroenterology. 2012; 143:1564–1575. e7. [PubMed: 22922013]

Fellous TG, Islam S, Tadrous PJ, Elia G, Kocher HM, Bhattacharya S, Mears L, Turnbull DM, Taylor RW, Greaves LC, et al. Locating the stem cell niche and tracing hepatocyte lineages in human liver. Hepatology. 2009; 49:1655–1663. [PubMed: 19309719]

Fleming KE, Wanless IR. Glutamine synthetase expression in activated hepatocyte progenitor cells and loss of hepatocellular expression in congestion and cirrhosis. Liver Int. 2013; 33:525–534. [PubMed: 23362937]

Forbes SJ, Gupta S, Dhawan A. Cell therapy for liver disease: From liver transplantation to cell factory. J. Hepatol. 2015; 62:S157–S169. [PubMed: 25920085]

Fujii M, Shibazaki Y, Wakamatsu K, Honda Y, Kawauchi Y, Suzuki K, Arumugam S, Watanabe K, Ichida T, Asakura H, Yoneyama H. A murine model for non-alcoholic steatohepatitis showing evidence of association between diabetes and hepatocellular carcinoma. Med. Mol. Morphol. 2013; 46:141–152. [PubMed: 23430399]

Furuyama K, Kawaguchi Y, Akiyama H, Horiguchi M, Kodama S, Kuhara T, Hosokawa S, Elbahrawy A, Soeda T, Koizumi M, et al. Continuous cell supply from a Sox9-expressing progenitor zone in adult liver, exocrine pancreas and intestine. Nat. Genet. 2011; 43:34–41. [PubMed: 21113154]

Grompe M. Liver stem cells, where art thou? Cell Stem Cell. 2014; 15:257–258. [PubMed: 25192457]

Grompe M, Lindstedt S, al-Dhalimy M, Kennaway NG, Papaconstantinou J, Torres-Ramos CA, Ou CN, Finegold M. Pharmacological correction of neonatal lethal hepatic dysfunction in a murine model of hereditary tyrosinaemia type I. Nat. Genet. 1995; 10:453–460. [PubMed: 7545495]

He G, Dhar D, Nakagawa H, Font-Burgada J, Ogata H, Jiang Y, Shala-pour S, Seki E, Yost SE, Jepsen K, et al. Identification of liver cancer progenitors whose malignant progression depends on autocrine IL-6 signaling. Cell. 2013; 155:384–396. [PubMed: 24120137]

Huch M, Dorrell C, Boj SF, van Es JH, Li VS, van de Wetering M, Sato T, Hamer K, Sasaki N, Finegold MJ, et al. In vitro expansion of single Lgr5+ liver stem cells induced by Wnt-driven regeneration. Nature. 2013; 494:247–250. [PubMed: 23354049]

Huch M, Gehart H, van Boxtel R, Hamer K, Blokzijl F, Verstegen MM, Ellis E, van Wenum M, Fuchs SA, de Ligt J, et al. Long-term culture of genome-stable bipotent stem cells from adult human liver. Cell. 2015; 160:299–312. [PubMed: 25533785]

Hui L, Bakiri L, Mairhorfer A, Schweifer N, Haslinger C, Kenner L, Komnenovic V, Scheuch H, Beug H, Wagner EF. p38alpha suppresses normal and cancer cell proliferation by antagonizing the JNK-c-Jun pathway. Nat. Genet. 2007; 39:741–749. [PubMed: 17468757]

Isse K, Lesniak A, Grama K, Maier J, Specht S, Castillo-Rama M, Lunz J, Roysam B, Michalopoulos G, Demetris AJ. Preexisting epithelial diversity in normal human livers: a tissue-tethered cytometric analysis in portal/periportal epithelial cells. Hepatology. 2013; 57:1632–1643. [PubMed: 23150208]

Jungermann K, Katz N. Functional specialization of different hepatocyte populations. Physiol. Rev. 1989; 69:708–764. [PubMed: 2664826]

Kaneko K, Kamimoto K, Miyajima A, Itoh T. Adaptive remodeling of the biliary architecture underlies liver homeostasis. Hepatology. 2015; 61:2056–2066. [PubMed: 25572923]

Kang JS, Wanibuchi H, Morimura K, Gonzalez FJ, Fukushima S. Role of CYP2E1 in diethylnitrosamine-induced hepatocarcinogenesis in vivo. Cancer Res. 2007; 67:11141–11146. [PubMed: 18056438]

Karin M. Nuclear factor-kappaB in cancer development and progression. Nature. 2006; 441:431–436. [PubMed: 16724054]

Kisseleva T, Gigante E, Brenner DA. Recent advances in liver stem cell therapy. Curr. Opin. Gastroenterol. 2010; 26:395–402. [PubMed: 20495456]

Kuraishy A, Karin M, Grivennikov SI. Tumor promotion via injury- and death-induced inflammation. Immunity. 2011; 35:467–477. [PubMed: 22035839]

Kuwahara R, Kofman AV, Landis CS, Swenson ES, Barendswaard E, Theise ND. The hepatic stem cell niche: identification by label-retaining cell assay. Hepatology. 2008; 47:1994–2002. [PubMed: 18454509]

Lavin Y, Winter D, Blecher-Gonen R, David E, Keren-Shaul H, Merad M, Jung S, Amit I. Tissue-resident macrophage enhancer landscapes are shaped by the local microenvironment. Cell. 2014; 159:1312–1326. [PubMed: 25480296]

Luedde T, Beraza N, Kotsikoris V, van Loo G, Nenci A, De Vos R, Roskams T, Trautwein C, Pasparakis M. Deletion of NEMO/IKK-gamma in liver parenchymal cells causes steatohepatitis and hepatocellular carcinoma. Cancer Cell. 2007; 11:119–132. [PubMed: 17292824]

Maeda S, Kamata H, Luo JL, Leffert H, Karin M. IKKbeta couples hepatocyte death to cytokine-driven compensatory proliferation that promotes chemical hepatocarcinogenesis. Cell. 2005; 121:977–990. [PubMed: 15989949]

Malato Y, Naqvi S, Schürmann N, Ng R, Wang B, Zape J, Kay MA, Grimm D, Willenbring H. Fate tracing of mature hepatocytes in mouse liver homeostasis and regeneration. J. Clin. Invest. 2011; 121:4850–4860. [PubMed: 22105172]

Michalopoulos GK. Liver regeneration. J. Cell. Physiol. 2007; 213:286–300. [PubMed: 17559071]

Miyajima A, Tanaka M, Itoh T. Stem/progenitor cells in liver development, homeostasis, regeneration, and reprogramming. Cell Stem Cell. 2014; 14:561–574. [PubMed: 24792114]

Nakagawa H, Hikiba Y, Hirata Y, Font-Burgada J, Sakamoto K, Hayakawa Y, Taniguchi K, Umemura A, Kinoshita H, Sakitani K, et al. Loss of liver E-cadherin induces sclerosing cholangitis and promotes carcinogenesis. Proc. Natl. Acad. Sci. USA. 2014a; 111:1090–1095. [PubMed: 24395807]

Nakagawa H, Umemura A, Taniguchi K, Font-Burgada J, Dhar D, Ogata H, Zhong Z, Valasek MA, Seki E, Hidalgo J, et al. ER stress cooperates with hypernutrition to trigger TNF-dependent spontaneous HCC development. Cancer Cell. 2014b; 26:331–343. [PubMed: 25132496]

Richardson MM, Jonsson JR, Powell EE, Brunt EM, Neuschwander-Tetri BA, Bhathal PS, Dixon JB, Weltman MD, Tilg H, Moschen AR, et al. Progressive fibrosis in nonalcoholic steatohepatitis: association with altered regeneration and a ductular reaction. Gastroenterology. 2007; 133:80–90. [PubMed: 17631134]

Rodrigo-Torres D, Affò S, Coll M, Morales-Ibanez O, Millán C, Blaya D, Alvarez-Guaita A, Rentero C, Lozano JJ, Maestro MA, et al. The biliary epithelium gives rise to liver progenitor cells. Hepatology. 2014; 60:1367–1377. [PubMed: 24700364]

Roskams T. Liver stem cells and their implication in hepatocellular and cholangiocarcinoma. Oncogene. 2006; 25:3818–3822. [PubMed: 16799623]

Sakurai T, He G, Matsuzawa A, Yu GY, Maeda S, Hardiman G, Karin M. Hepatocyte necrosis induced by oxidative stress and IL-1 alpha release mediate carcinogen-induced compensatory proliferation and liver tumorigenesis. Cancer Cell. 2008; 14:156–165. [PubMed: 18691550]

Schaub JR, Malato Y, Gormond C, Willenbring H. Evidence against a stem cell origin of new hepatocytes in a common mouse model of chronic liver injury. Cell Rep. 2014; 8:933–939. [PubMed: 25131204]

Schmelzer E, Zhang L, Bruce A, Wauthier E, Ludlow J, Yao HL, Moss N, Melhem A, McClelland R, Turner W, et al. Human hepatic stem cells from fetal and postnatal donors. J. Exp. Med. 2007; 204:1973–1987. [PubMed: 17664288]

Sell S, Leffert HL. Liver cancer stem cells. J. Clin. Oncol. 2008; 26:2800–2805. [PubMed: 18539957]

Slack JM. Metaplasia and transdifferentiation: from pure biology to the clinic. Nat. Rev. Mol. Cell Biol. 2007; 8:369–378. [PubMed: 17377526]

Tanimizu N, Nishikawa Y, Ichinohe N, Akiyama H, Mitaka T. Sry HMG box protein 9-positive (Sox9+) epithelial cell adhesion molecule-negative (EpCAM-) biphenotypic cells derived from hepatocytes are involved in mouse liver regeneration. J. Biol. Chem. 2014; 289:7589–7598. [PubMed: 24482234]

Tarlow BD, Finegold MJ, Grompe M. Clonal tracing of Sox9+ liver progenitors in mouse oval cell injury. Hepatology. 2014a; 60:278–289. [PubMed: 24700457]

Tarlow BD, Pelz C, Naugler WE, Wakefield L, Wilson EM, Finegold MJ, Grompe M. Bipotential adult liver progenitors are derived from chronically injured mature hepatocytes. Cell Stem Cell. 2014b; 15:605–618. [PubMed: 25312494]

Tomasetti C, Vogelstein B. Cancer etiology. Variation in cancer risk among tissues can be explained by the number of stem cell divisions. Science. 2015; 347:78–81. [PubMed: 25554788]

Weglarz TC, Degen JL, Sandgren EP. Hepatocyte transplantation into diseased mouse liver. Kinetics of parenchymal repopulation and identification of the proliferative capacity of tetraploid and octaploid hepatocytes. Am. J. Pathol. 2000; 157:1963–1974. [PubMed: 11106569]

Wong FW, Chan WY, Lee SS. Resistance to carbon tetrachlo-ride-induced hepatotoxicity in mice which lack CYP2E1 expression. Toxicol. Appl. Pharmacol. 1998; 153:109–118. [PubMed: 9875305]

Yanger K, Zong Y, Maggs LR, Shapira SN, Maddipati R, Aiello NM, Thung SN, Wells RG, Greenbaum LE, Stanger BZ. Robust cellular reprogramming occurs spontaneously during liver regeneration. Genes Dev. 2013; 27:719–724. [PubMed: 23520387]

Yanger K, Knigin D, Zong Y, Maggs L, Gu G, Akiyama H, Pikarsky E, Stanger BZ. Adult hepatocytes are generated by self-duplication rather than stem cell differentiation. Cell Stem Cell. 2014; 15:340–349. [PubMed: 25130492]

Highlights

- Hybrid hepatocytes (HybHP) constitutively reside in portal triads of healthy liver
- HybHP can replenish the entire parenchyma after chronic hepatocyte damage
- Despite multiple divisions, HybHP do not originate HCC in three independent models
- HybHP exhibit unmatched regenerative capacity in a diseased liver

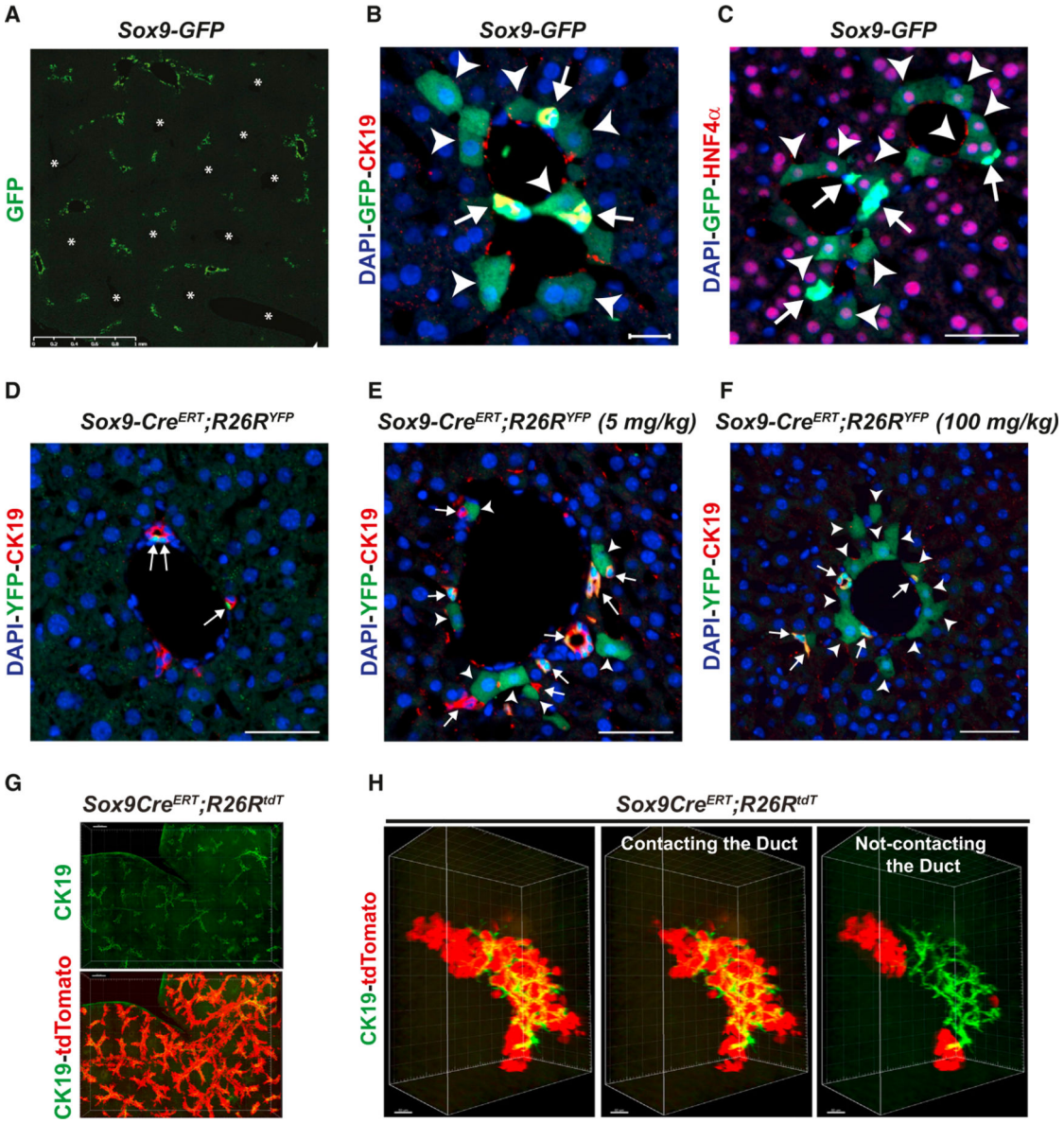

Figure 1. Hybrid Periportal Hepatocytes that Express *Sox9-GFP* and HNF4α

(A–C) Liver sections from 3-month-old *Sox9-GFP* males were analyzed by immunofluorescence (IF) microscopy. (A) A portion of a whole slide scan showing GFP^+ cells around portal areas. Asterisks—central veins. Scale bar, 1 mm. (B and C) Liver sections from above mice were stained with DAPI, GFP, CK19, and HNF4α antibodies and imaged. Ductal cells ($CK19^+$, $HNF4α^-$; arrows) show a strong GFP signal. A weaker GFP signal is exhibited by a few periportal $CK19^-$, $HNF4α^+$ hepatocytes (arrowheads).

(D) Liver sections from 3-month-old *Sox9-Cre^{ERT};R26R^{YFP}* mice were examined for YFP and CK19 expression and counterstained with DAPI. A few ductal $CK19^+$ cells express YFP spontaneously without tamoxifen treatment (arrows).

(E) Liver sections of *Sox9-Cre^{ERT};R26R^{YFP}* mice treated with tamoxifen (5 mg/kg) were analyzed as above. Ductal $CK19^+$ cells (arrows) and a few periportal hepatocytes (arrowheads) are YFP labeled.

(F) The same mice were given 100 mg/kg of tamoxifen and analyzed as above. $CK19^{-}$ hepatocytes (arrowheads) are YFP labeled. Ductal $CK19^{+}$, YFP^{+} cells (arrows) are shown. Bracketed scale bar, 20 μm; open scale bar, 50 μm.

(G) Three-dimensional reconstruction of dTomato fluorescence in a clarified liver from a tamoxifen-treated *Sox9-Cre^{ERT};R26R^{tdTomato}* mouse (red channel). Ductal cells were stained for CK19 (green channel). Scale bar, 500 μm.

(H) Three-dimensional reconstruction of a PT from (G), in which HybHP that either contact duct cells or are located ≥ one cell diameter away are shown. Scale bar, 50 μm.

See also Figure S1 and Movies S1, S2, S3, S4, and S5.

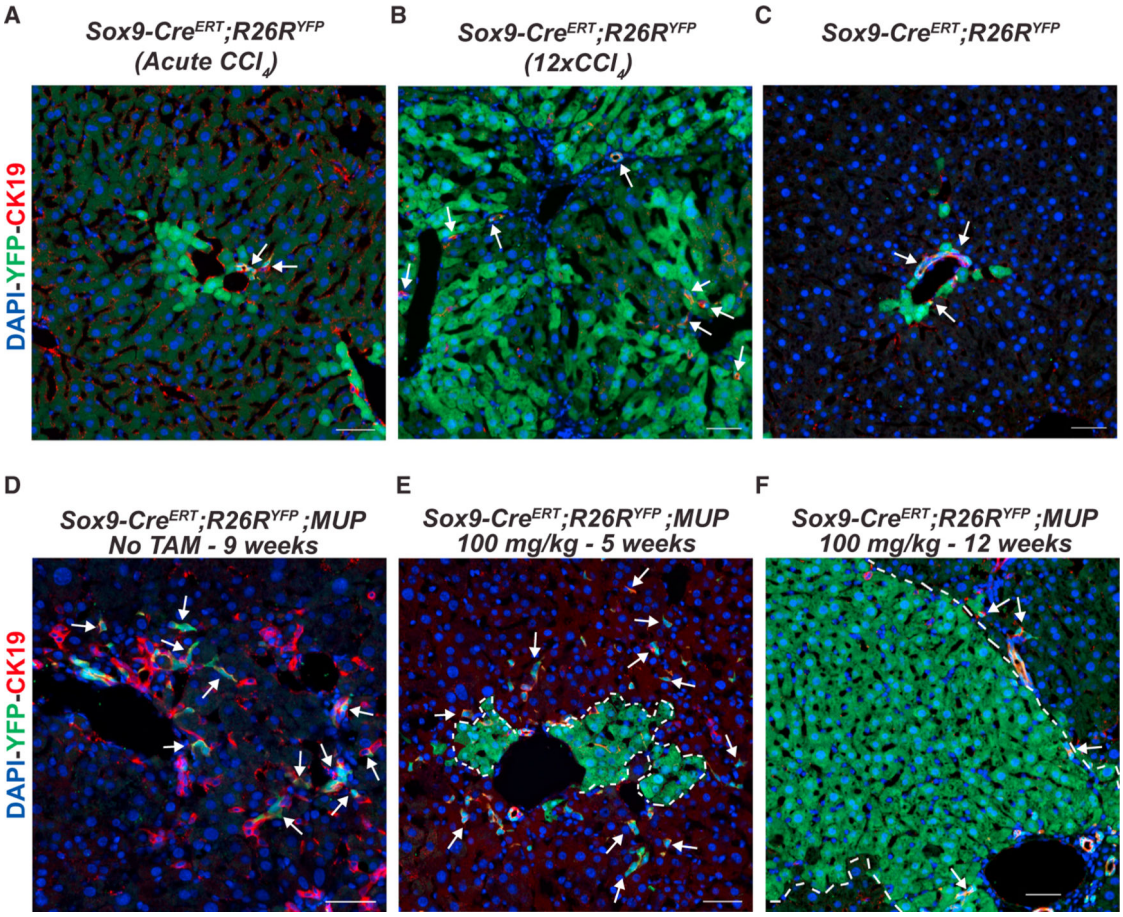

Figure 2. HybHP Make Major Contribution to Parenchymal Restoration after Chronic Hepatocyte Damage

(A) Acute CCl administration to *Sox9-Cre^{ERT};R26R^{YFP}* mice previously injected with tamoxifen (100 mg/kg). Livers were analyzed as in Figure 1.

(B) Tamoxifen (100 mg/kg)-injected *Sox9-Cre^{ERT};R26R^{YFP}* mice (8 weeks old) received two weekly CCl_4 injections for 6 weeks. Livers were excised and analyzed as above.

(C) Same as in (B) but without CCl_4 treatment.

(D) *Sox9-Cre^{ERT};R26R^{YFP};MUP-uPA* mice (9 weeks old) were analyzed. 99.9% YFP$^+$-labeled (green) cells are ductal/oval CK19$^+$ cells (red).

(E and F) *Sox9-Cre^{ERT};R26R^{YFP};MUP-uPA* mice were injected with 100 mg/kg tamoxifen at P10 and analyzed as above at 5 weeks (2 weeks after damage onset) (E) or 12 weeks (F). Arrows, ductal cells (CK19$^+$, red). Scale bar, 50 μm. See also Figures S2 and S3.

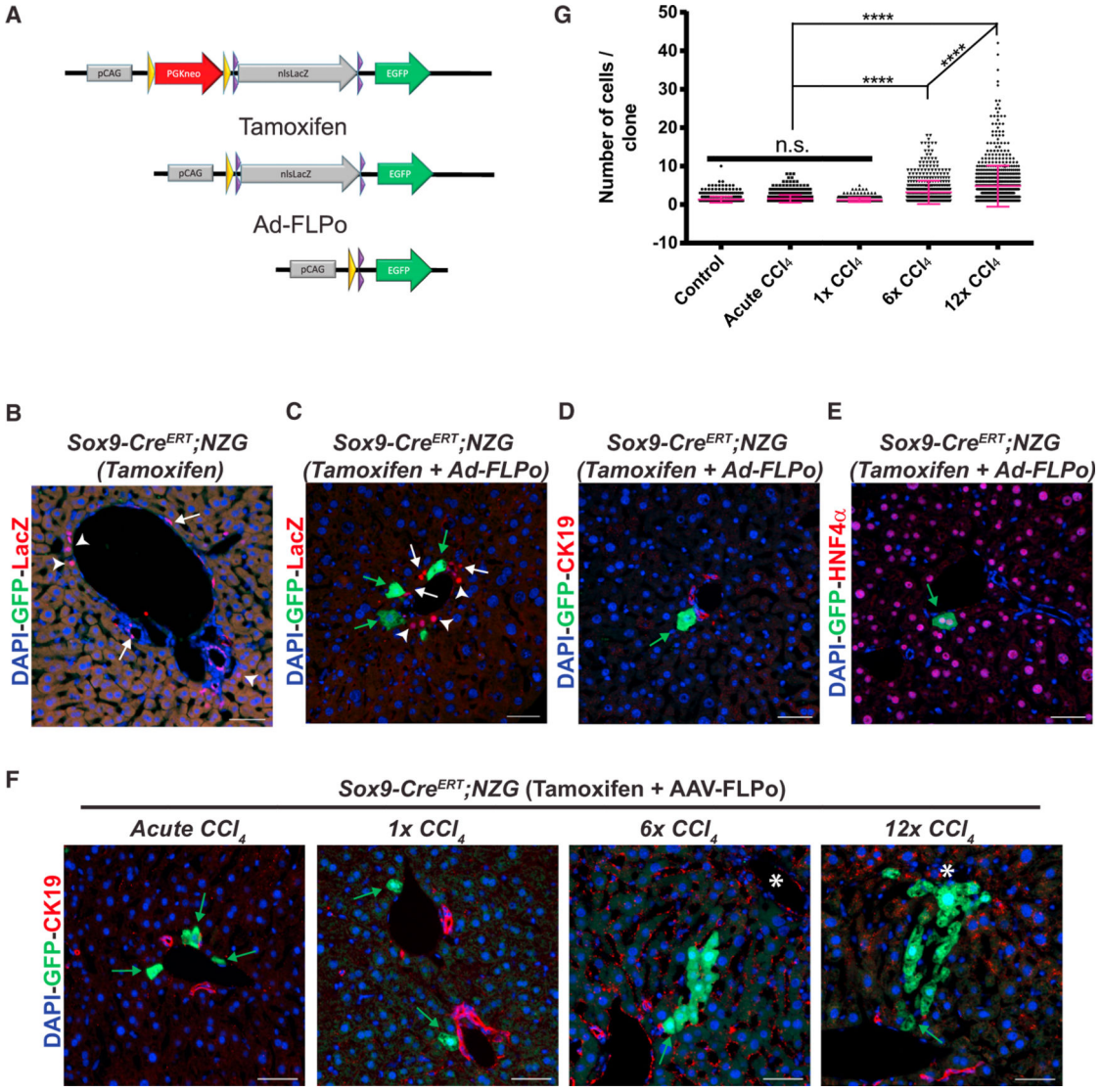

Figure 3. Clonal Labeling Confirms HybHP Role in Liver Injury Repair

(A) A scheme outlining clonal labeling of HybHP with dual recombinase *NZG* reporter.

(B) *Sox9-Cre^{ERT};NZG* mice (4–6 weeks old) were injected with 100 mg/kg of tamoxifen and 10 days later given 20 mg/kg tamoxifen. Ductal cells and HybHP were positive for nuclear LacZ (arrows and arrowheads, respectively).

(C–E) *Sox9-Cre^{ERT};NZG* mice (4–6 weeks old) were first treated with tamoxifen as above and then given 10^9 or 5×10^{11} Adeno- or AAV-FLPo viral particles, respectively. After 2 weeks, liver sections were imaged. Some HybHP were GFP$^+$ and nuclear LacZ$^-$ (green arrows) (C). GFP$^+$ HybHP were CK19$^-$ (D) and HNF4α$^+$ (E).

(F) *Sox9-Cre^{ERT};NZG* mice were given tamoxifen followed by AAV-FLPo and challenged with either high CCl_4 (acute) or 1, 6, or 12 low CCl_4 doses (chronic). Livers were excised and analyzed as in (D).

(G) Quantification of the cell number per clone in each experimental group. No treatment: 750 independent clones, n = 3; acute CCl_4: 939 independent clones, n = 3; 1 low dose: 469 independent clones, n = 3; 6 low doses, 626 independent clones, n = 3; 12 low doses: 756

independent clones, n = 4. ****p value < 0.0001 based on a one-way ANOVA with multiple comparisons. Scale bar, 50 μm. Mean and SD are shown. Asterisks: central veins. n.s.: not significant.

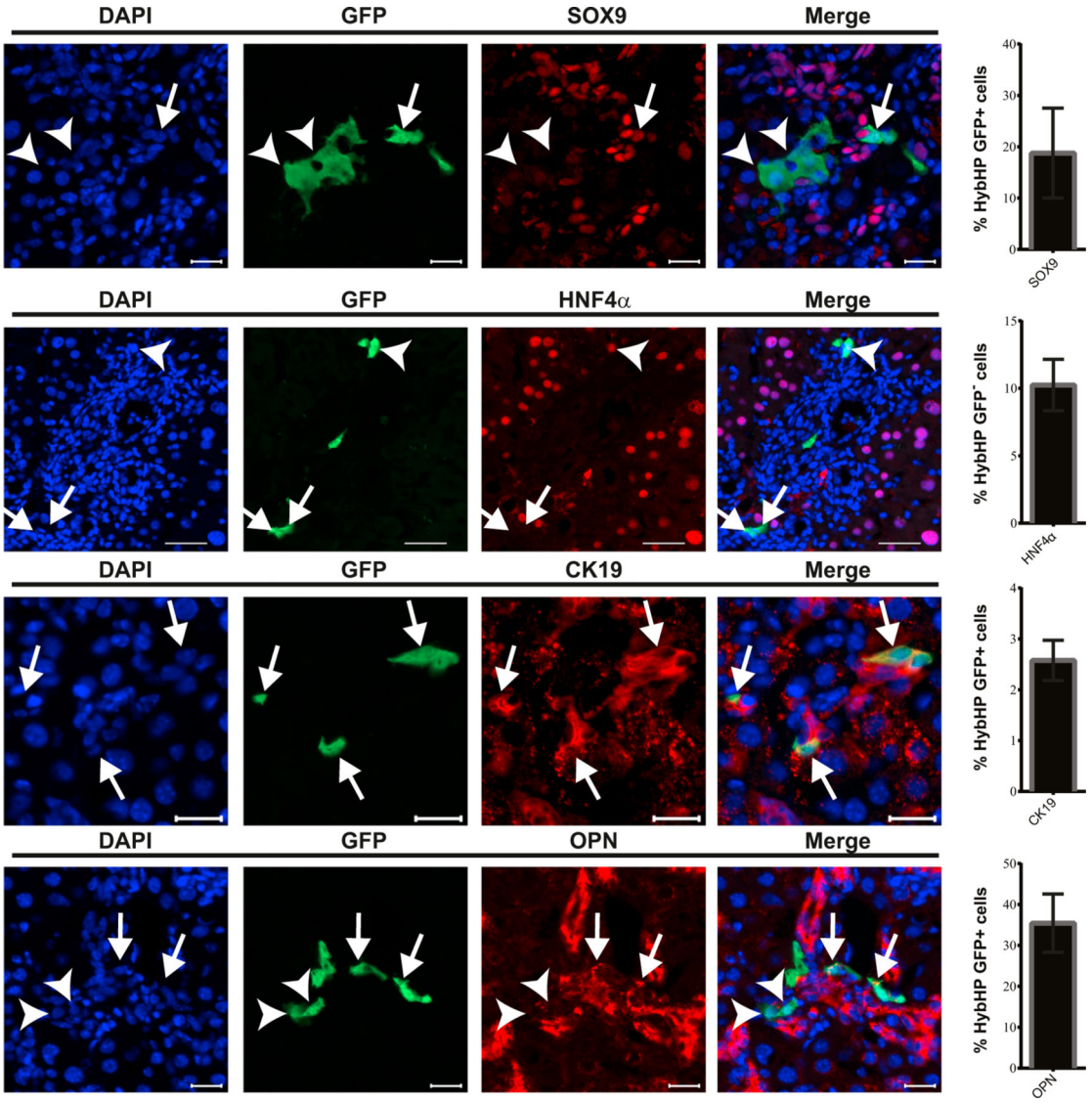

Figure 4. HybHP Can Generate Ductal Cells upon Cholestatic Injury

Sox9-Cre^{ERT}*;NZG* mice were given tamoxifen and Adeno-FLPo as in Figure 3 and placed on DDC diet 3 weeks later. After 6 weeks on diet, the fate of HybHP was analyzed by co-staining for OPN, SOX9, HNF4α, and CK19. Arrows depict HybHP positive for ductal markers (SOX9, OPN, and CK19) or negative for HNF4α. Arrowheads denote HybHP negative for ductal markers or positive for HNF4α. Graphs show percentages of GFP^{+} HybHP positive for CK19 (n = 1,260), SOX9 (n = 513), or OPN (n = 994) and negative for HNF4α (n = 676) in three independent mice. In non-treated mice (n = 3), no GFP^{+} HybHP that were positive for CK19 (n = 551) or SOX9 (n = 232) or negative for HNF4α (n = 323) were found. Only 0.72% of GFP^{+} HybHP were OPN positive (n = 556). Bracketed and open scale bars: 20 μm and 50 μm, respectively. Mean and SD are shown.

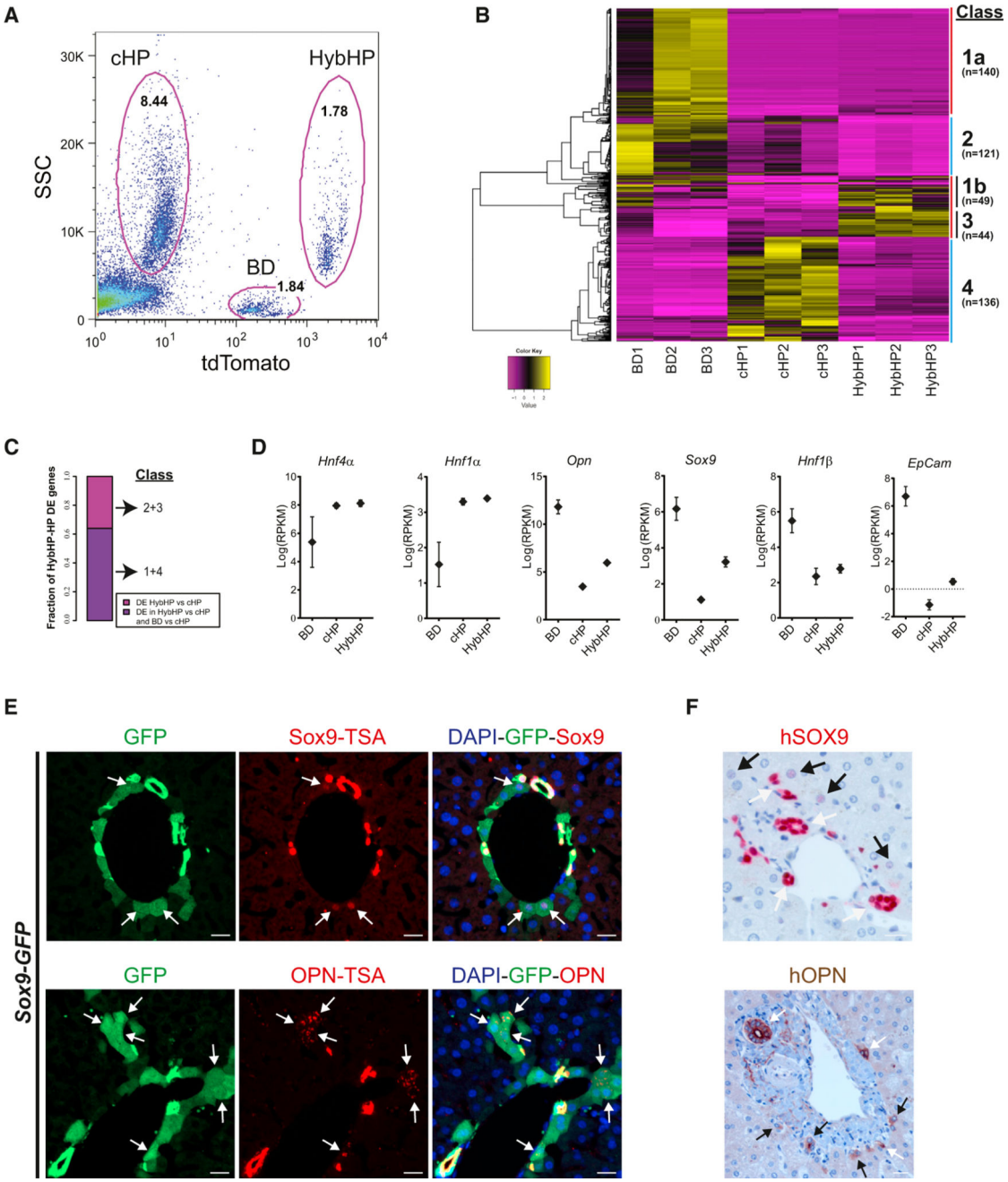

Figure 5. The HybHP Transcriptome Confirms Their Hybrid Character

(A) cHP, BD, and HybHP from a collagenase digest of a *Sox9-Cre*^{ERT}*;R26R*^{tdTomato} liver (mice were treated with 100 mg/kg of tamoxifen and 10 days later given 20 mg/kg tamoxifen) were FACS separated after excluding dead cells and doublets and gating based on size/granularity (FCS/SSC) and tdTomato expression.

(B) Total cellular RNA was extracted from the three populations (three independent isolations) and deep sequenced. Shown is a heatmap of genes that were differentially expressed between HybHP and cHP.

(C) Proportions of genes from above that are differentially expressed between HybHP and cHP and that show the same expression trend in BD versus cHP or not.
(D) Normalized expression values (in reads per kilobase per million) of the indicated genes in HybHP, cHP, and BD. Mean and SD are shown.
(E) IF analysis using Tyramide Signal Amplification (TSA) of Sox9-GFP transgenic mouse liver sections stained for SOX9 and OPN. Arrows: HybHP with weak SOX9 and OPN expression.
(F) Normal human liver sections stained for SOX9 and OPN.
Black arrows: periportal hepatocytes with weak expression of SOX9 or OPN. White arrows: ductal cells. Scale bars, 20 μm. See also Figures S4, S5, and S6.

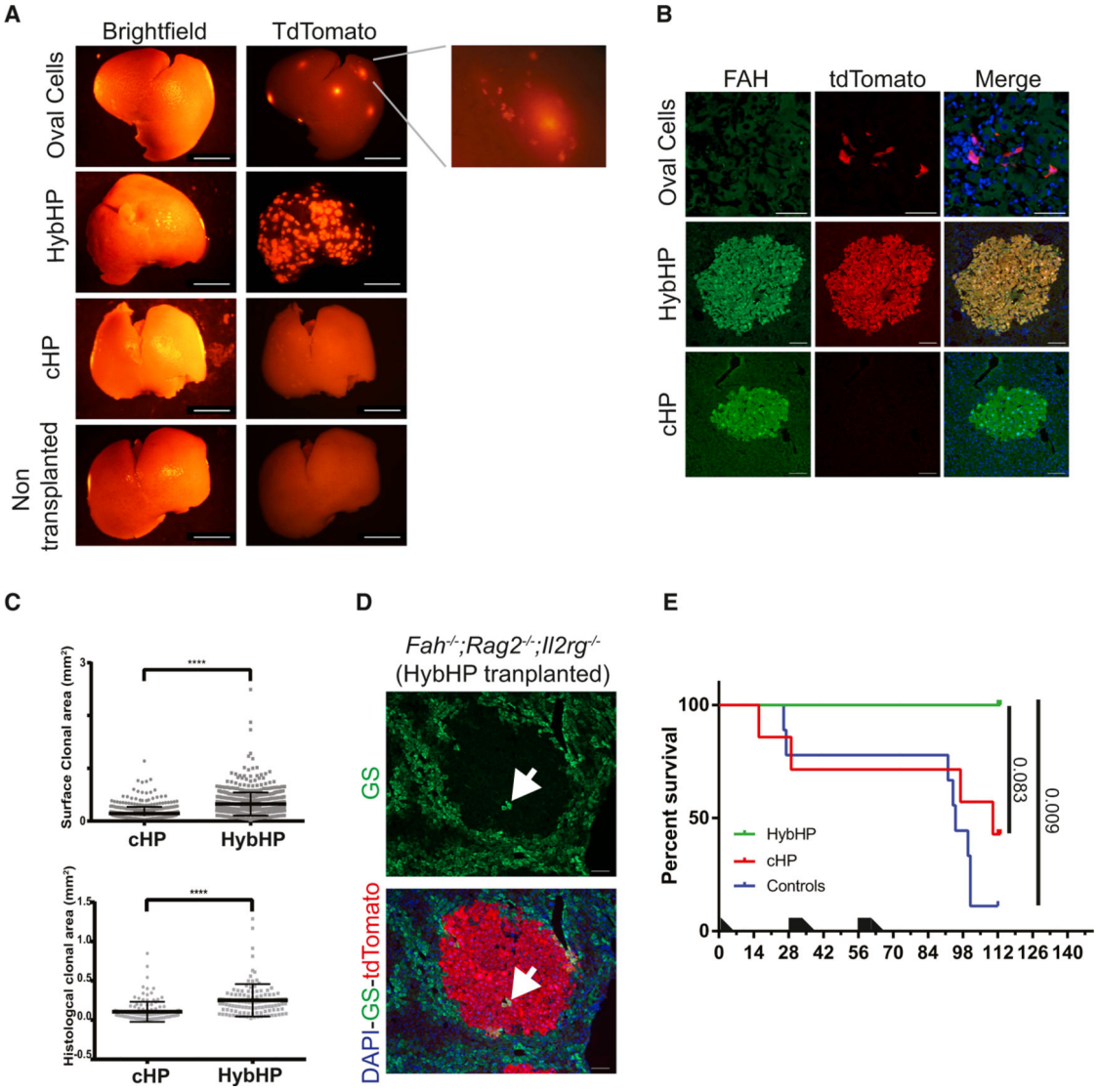

Figure 6. HybHP Exhibit Higher Repopulation Capacity than cHP or Oval Cells

(A) HybHP and cHP were FACS sorted from *Sox9-Cre^{ERT};R26R^{tdTomato}* mice (8–12 weeks old treated with 100 mg/kg of tamoxifen and 10 days later given 20 mg/kg tamoxifen), and 45,000 cells were transplanted into *Fah$^{-/-}$;Rag2$^{-/-}$;Il2rg$^{-/-}$* mice (n = 3 for cHP and n = 2 for HybHP). Oval cells (OC; 45,000) were obtained by FACS sorting from a *Sox9-Cre^{ERT};R26R^{tdTomato}* mouse fed with CDE diet for 3 weeks and transplanted into three *Fah$^{-/-}$;Rag2$^{-/-}$;Il2rg$^{-/-}$* mice. Bright-field and tdTomato images of the medial lobes of non-transplanted and transplanted livers 8 weeks after transplantation. Scale bars, 5 mm.

(B) Frozen sections of above livers were analyzed by direct fluorescence for tdTomato and IF for FAH expression.

(C) Upper graph: Surface clonal area quantification in three cHP- and two HybHP-transplanted livers. OC clones were not quantified due to their small number and size. **** = unpaired t test with Welch's correction $p < 0.0001$. cHP clones, n = 500 and HybHP clones, n = 695. Every measured clone with the mean and SD is shown. Lower graph: areas of all clones in liver sections from (B). **** = unpaired t test with Welch's correction p <

0.0001. cHP clones, n = 132 and HybHP clones, n = 113. Every measured clone with mean and SD is shown.

(D) Liver sections from HybHP-transplanted mice in (B) stained for GS. White arrow: tdTomato^{+} GS^{+} HybHP. Scale bar, 100 μm.

(E) Survival of an independent cohort of mice transplanted with HybHP (n = 4), cHP (n = 7), or non-transplanted controls (n = 9). p values were determined by log-rank (Mantel-Cox) test. Black polygons over x axis represent periods while the animals were on NTBC during the on-off NTBC cycles.

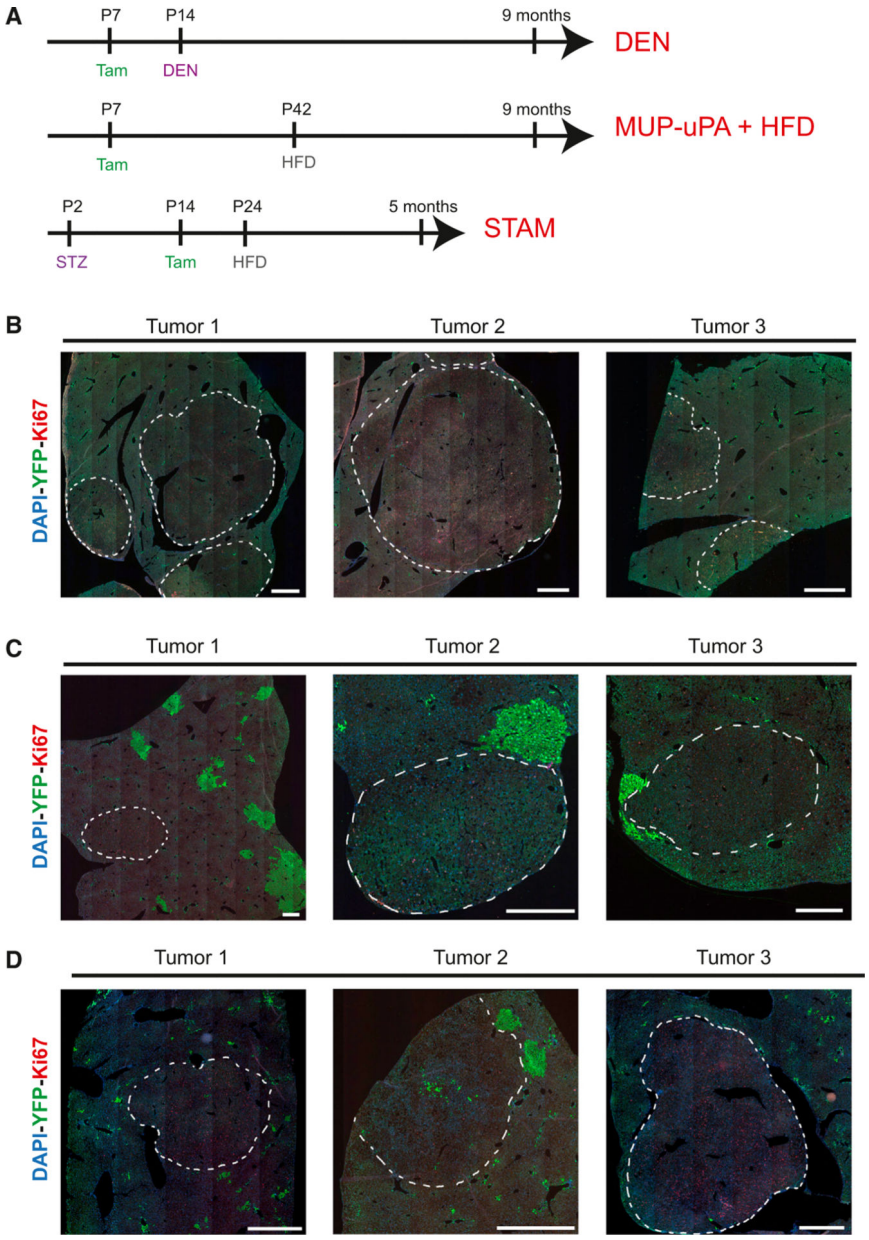

Figure 7. Neither HybHP nor Oval Cells Preferentially Give Rise to HCC

(A) Experimental design for HybHP and OC line-age tracing in three different HCC models using *Sox9-Cre^{ERT};R26R^{YFP}* or *Sox9-Cre^{ERT};R26-R^{YFP};MUP-uPA* mice.

(B–D) Ki67 IF and morphology were examined to locate tumor nodules (delineated by a dashed line) in whole slide scans. None of the tumor areas contained YFP^{+} cancer cells. Three representative examples are shown for each HCC model (A-DEN, B-MUP-uPA + HFD, and C-STAM). Scale bars, 0.5 mm (C); 1 mm (B and D).

See also Figure S7.